

Benchmarking the ability of a controller to execute quantum error corrected non-Clifford circuits

Yaniv Kurman¹, Lior Ella¹, Ramon Szmuk¹, Oded Wertheim¹, Benedikt Dorschner², Sam Stanwyck², and Yonatan Cohen¹

¹Quantum Machines Inc., Tel Aviv, Israel

²NVIDIA Corp, Santa Clara, CA, USA

Corresponding author: Yaniv Kurman (email: yanivk@quantum-machines.co).

ABSTRACT Reaching useful fault-tolerant quantum computation relies on successfully implementing quantum error correction (QEC). In QEC, quantum gates and measurements are performed to encode quantum logic in a spatially nonlocal wavefunction within an error protected Hilbert space. To reach protected logic, classical processing is used to decode the measurements into estimated local errors and eventually logical errors. To date, QEC research has concentrated on developing and evaluating QEC codes and decoding algorithms. In this work, we elucidate that the feasibility of an error corrected non-Clifford circuits hinges upon the classical control system running the QEC codes. In particular, QEC controllers need to perform a key task: decoding-based feed-forward with low latency, defined as the time between the last measurement to be decoded and a mid-circuit quantum operation that depends on it. We analyze how the QEC control system latency performance determines the operation regime of a QEC circuit: latency divergence, classical-controller limited runtime, or quantum-operation limited runtime. This, in turn, implies that any control system intended to execute QEC will need to be evaluated on its ability to perform low-latency decoding-based feed-forward. We define here two near-term benchmarks that evaluate this ability, thus quantifying the potential of holistic QEC controller-decoder systems to successfully execute QEC. These benchmarks and analysis set a standard for evaluating and developing QEC control systems toward their realization as a main component in fault-tolerant quantum computation.

I. INTRODUCTION

Quantum error correction (QEC) [1], [2] stands as the clearest path for achieving the exponential advantage of quantum computing, enabling the resolution of significant problems such as simulating complex quantum systems [3], factorization[4], and more. In expected QEC implementations, quantum logic is encoded across several physically separated qubits, with repeated local parity measurements (stabilizer rounds) facilitating the detection and correction of local physical errors [5]. Although increasing the number of physical qubits introduce additional errors, this expansion can exponentially reduce logical quantum errors if the physical errors are below a certain QEC code-dependent threshold [6], [7], opening the path toward useful quantum computation.

The successful execution of QEC codes hinges on the performance of several key components. First is the performance of the qubits themselves, whose physical error rates should be sufficiently smaller than the QEC error threshold. Secondly, the quantum controller which executes the quantum computation should perform all quantum gate operations with optimal fidelities. Thirdly, a successful QEC implementation requires a quantum error decoding unit

(decoder). The decoder maps the physical quantum measurements into quantum errors using a classical algorithmic procedure[8]. Since QEC decoding algorithms are significantly more complex than the current embedded classical processing in a quantum control unit [9], [10], [11], [12], [13], state-of-the-art QEC experiments still make use of independently developed quantum control and decoding units [14], [15].

To date, separate criteria are used to evaluate quantum control units[13], [16], and QEC decoders. Evaluation of quantum control units is centered around the analog output performance and parallel quantum-classical processing. Evaluation of the decoding hardware, on the other hand, focuses on achieving a shorter decoding time per stabilizer round than the time of the stabilizer round itself [17], a criteria that prevents a diverging decoding duration [18]. These separated evaluations, however, fail to answer the basic question of whether an integrated controller and decoder system can successfully execute QEC algorithms, and their overall performance in a realistic setting.

In this manuscript, we propose the first holistic benchmark for the performance of the full classical section of the quantum

computer, comprised of the controller, decoding, and their integration. To emphasize its holistic nature, we denote this part of the computer as a “controller-decoder unit” (CDU). Our benchmarks focus on the CDU’s ability to apply *decoding-based, low-latency, feed-forward* operations during circuit execution, where the feed-forward latency (FFL) is defined by the time interval between the pulse of a feed-forward gate (mid-circuit gate modification) and the last measurement it relies on. Our analysis shows how the evolution of the FFL during the QEC computation determines whether the CDU will reach a continuously increasing (diverging) latency value, thus rendering the quantum computer inoperable, or a steady-state FFL. The steady-state FFL is defined as an equilibrium point between the time it takes to decode a certain dataset and the time in which this to-be-decoded dataset is created. The steady-state FFL depends on the decoding time, the controller-decoder communication channel, and the controller’s operation speed. Moreover so, its value is a crucial performance metric since it determines the duration of a non-Clifford gate and its fidelity. Thus, our suggested benchmarks will verify the CDU’s capability to apply decoding-dependent quantum gates while parallelizing the decoding itself with quantum processing and evaluate the overall steady-state duration, under near-term settings with only one or two logical qubits.

Our manuscript is structured as follows. Section II serves as an introduction to QEC-based quantum computation with the well-known surface code. Section III presents the CDU as a control unit, which functions as the cornerstone for the execution of QEC-based quantum computations. Section IV elucidates the role of the FFL in QEC computation and shows how to determine its steady-state behavior using a dynamical system approach. In section V, we suggest two benchmarks, exemplified by simple logical operations, and evaluated given different system parameters. Finally, in section VI we discuss more benchmarks and the long-term requirements of a CDU once quantum hardware scales.

II. QEC QUANTUM COMPUTATION WITH SURFACE CODES

The surface code [19], [20] stands out among the different QEC codes because of its high error threshold of $\sim 1\%$, orders of magnitude higher than other codes, and simple physical requirements. Many aspects of the surface code have been developed in detail, including fault-tolerant computation techniques [21], [22], [23], [24], [25], [26], high-fidelity magic state preparation techniques [27], [28], [29], decoding algorithms [30], [31], [32], [33], [34], [35], [36], [17], simulation tools [37], distillation schemes [25], [38], [39], and scaling proposals [24], [25]. This motivates us to define, in section V, the CDU benchmarks with the surface codes as a representative example. Nevertheless, we keep in mind that the benchmarks below can be easily modified to any stabilizer code.

We start with a brief introduction to QEC quantum computation with the surface-code. The surface code implements each logical qubit with a set of parity checks that can be tiled onto a square lattice. In the qubit-efficient rotated surface implementation, the quantum information of a single qubit (logical qubit) is encoded in a single surface with d^2 physical qubits called data qubits (black circles in Figure 1a), where d is the distance of the QEC code. In addition to the data qubits, the logical qubit requires d^2-1 ancillary physical qubits which perform Pauli Z or Pauli X (blue and purple circles in Figure 1a, respectively) local parity measurements of their nearest-neighbor data qubits. These Pauli Z and Pauli X measurements track the presence of local bit or phase flip errors, respectively, on the data qubits. The $+1$ eigenstate of all measured Pauli operators define the Hilbert subspace of the logical qubit (called the code space) [5], which the data qubits collapse into up to a local bit or phase flip. This collapse to the code space is called stabilization, the Pauli operators that are probed are called stabilizers, and the act of probing is called a stabilizer round which is constantly repeated during all fault-tolerant logical quantum gates of the surface codes. For example, Figure 1b presents the required physical gate sequence that implements a multi-surface parity check (i.e., lattice-surgery) fault-tolerantly by repeating the QEC stabilizer round d times.

An established implementation of quantum information processing with QEC uses measurement-based quantum computation. The fault-tolerant logic gate-set includes single-logical-qubit (i.e., single-surface) measurements and initializations in the X or Z basis, as well as multi-logical-qubit parity measurements in the Z/X basis (e.g., ZZ, XX, ZX for two surfaces) [21], [24], [25], [26]. The commonality between all the above is that their physical implementation can be verified with (or implemented by) the QEC code’s stabilizers, where a padding of d stabilizer rounds before, after, or during the logical gate are needed for a fault-tolerant implementation. However, to complete to a universal gate set and reach quantum advantage (Gottesman-Knill theorem)[40], it is required to perform surface initialization in a logical magic-state, namely a state which is not a logical Pauli eigenstate. Such preparation is non-fault-tolerant and will eventually require magic state distillation [25], [38], [39].

Figure 1c illustrates a QEC computation example implementing a non-Clifford $T=\text{diag}(1, e^{i\pi/4})$ gate on a general qubit with state $|\psi\rangle$ using an ancillary surface initialized in the logical $|T\rangle=|0\rangle+e^{i\pi/4}|1\rangle$ magic-state. Each measurement outcome during the measurement-based computation has a 50% chance of being 0 or 1, which dictates a required logical-circuit modification. A correction within the Pauli group (X, Y, or Z) in the logical circuit can propagate in software without modifying the logical circuit (thus avoiding additional errors and delays), and therefore does not require logical circuit modifications [20]. However, a correction in the form of a logical $S=\text{diag}(1, i)$ gate cannot propagate through a non-commuting non-Clifford gate (as explained in SM section S1).

Consequently, feed-forward must be applied to implement a logical non-Clifford gate (in our example, if m_0 is 1), and moreover, it is decoding-dependent.

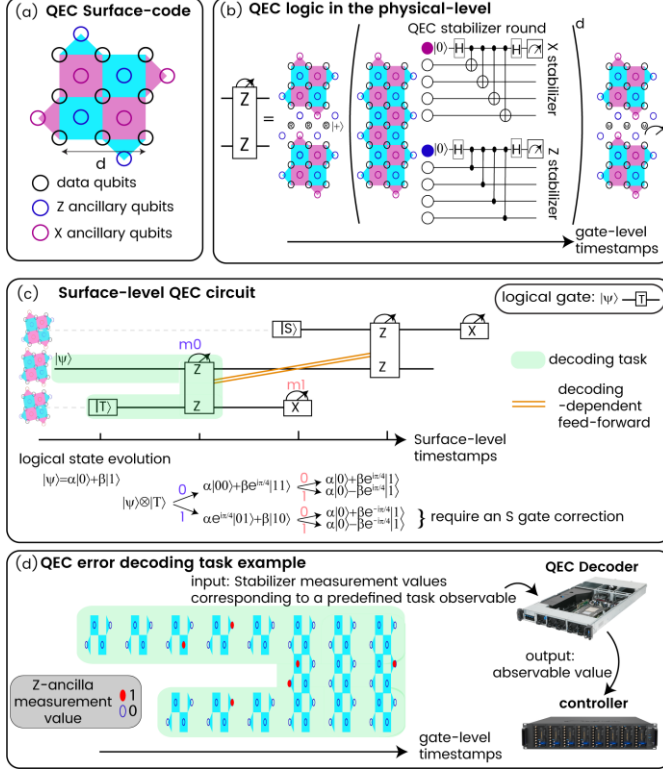


FIGURE 1. Example of non-Clifford QEC computation with surface codes. (a) A logical qubit in the surface code, implemented with d^2 data qubits (black) and d^2-1 ancilla qubits (blue and purple) which are used for the stabilizer measurements. (b) The physical-level QEC quantum circuit, which implements a logical ZZ parity measurement through initialization of data qubits which connect two surfaces, d repeated stabilizer rounds for the elongated surface, and measurement of the connecting data qubits. We note that this operation is fault-tolerant due to the d repetitions of the stabilizer round. (c) The surface level QEC circuit, which implements a single non-Clifford (T) gate. This is done, for example, using two ancillary surfaces and the native surface-level gates which implement fault-tolerantly measurement-based quantum computation. To implement a T gate rather than a T^{-1} (up to a Pauli Z correction), a logical feed-forward in the form of an S gate is needed, depending on the m_0 result, as we show in the logical state evolution. Decoding is required to find m_0 (decoding task marked in green), and thus the feed-forward (orange) which implements the S gate (using a $|i\rangle=|0\rangle+i|1\rangle$ state) is decoding-dependent. (d) An example of the decoding task in (c) for a $d=3$ code. The stabilizer measurement results (Z-stabilizers) which correspond to the logical measurement outcome of interest (logical ZZ parity measurements) are sent to a QEC decoder which determines and sends to the controller its best estimation to the logical measurement value.

The effectiveness of QEC in reducing logical errors depends on accurate error decoding. Decoding is a classical algorithmic process that analyzes all physical measurements acquired up to a certain point and converts this data into logical measurement outcomes and logical Pauli corrections for the corresponding logical qubits. Decoding during the evolution of the circuit is essential because some Pauli errors cannot propagate through non-Clifford gates without transforming into non-Clifford errors (see SI section S1). Therefore, it is crucial to track physical errors within logical qubits on-line to implement correct quantum logic. The field of decoding algorithms is under intense research [17] with available algorithms exhibiting trade-offs between high accuracy [32],

speed [33], scalability [34], and potential for implementation in available hardware [41]. Figure 1d demonstrates a decoding procedure. The decoder's input includes all physical measurements that can track an error in a logical measurement outcome (in this case, an error in the ZZ multi-qubit measurement from Figure 1c), and the output is the logical measurement value, possibly accompanied by additional metadata such as logical qubit Pauli frame flips (I, X, Y, or Z). The decoder's output is then sent to the quantum control unit, which executes the physical implementation of decoding-dependent logical gates.

One of the greatest challenges in performing QEC computation is achieving low latencies for decoding-dependent feed-forward, i.e., minimizing the time from the physical execution of a logical measurement to the time the controller issues a conditional pulse based on the decoded logical measurement outcome. This challenge motivates the transition from viewing the decoder and controller separately to adopting a holistic perspective on a CDU.

III. THE CDU

We define the controller-decoder unit (CDU) as a classical hardware element designed to enable full execution of QEC quantum computation. The CDU must conform to several requirements: (i) executing QEC quantum gate sequences via analog signals to the quantum processors, (ii) performing error decoding, and (iii) integrating the controller and decoder to execute quantum gates based on decoding outcomes. Importantly, we do not limit the CDU to any specific quantum hardware, classical hardware implementation, QEC code, decoding algorithm, micro-architecture, or controller-decoder communication protocol.

Figure 2 illustrates the central role of the CDU in QEC quantum computation. Before execution (offline), it is essential to define the CDU tasks, which include the QEC code, the target quantum logical gate-level circuit, the decoding algorithm, and the physical description of the quantum computer. This information is compiled into a set of inputs for the CDU. The quantum controller receives the pulse-level circuit to run on the quantum processing unit (QPU), including optimized pulse sequences, classical decision-making, and decoding-dependent conditional gates. The CDU's decoder receives the expected data transfer, parameters such as the matching graph dimensions, which can be static or dynamic. Once all components of the CDU are ready, circuit execution begins (runtime). Physical quantum measurement results (ancillary and data-qubit measurements) are sent to the decoder, which returns logical frames and logical measurement results to the controller and the user. The

benchmarks below aim to verify the CDU ability to perform these tasks.

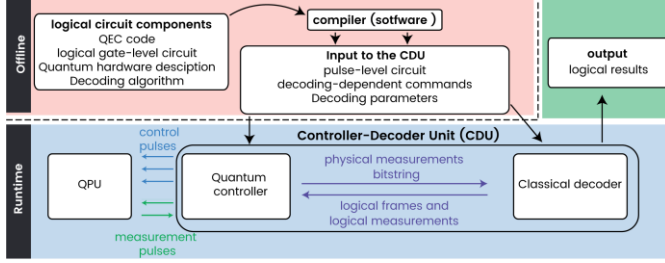


FIGURE 2. The CDU's central role in QEC quantum computation. The CDU is a runtime hardware component which includes both the classical decoder and the quantum controller that directly interacts with quantum processing unit (QPU). Here we show an implementation for running a QEC logical circuits: an offline software compiler converts the QEC code, logical gate-level circuit, quantum hardware description, and decoding algorithm into the input of the CDU: a pulse-level circuit and decoding parameters. During runtime, the physical circuit is executed by the CDU with syndrome flow from the controller to the decoder while the decoding results, in the form of logical measurement results and logical frames, are both returned to the quantum controller and sent to the user.

Current quantum control units can already fulfill most of their requirements due to their flexibility in executing quantum logic with mid-circuit control flow capabilities such as conditional commands, loops, and other branching at nanosecond timescales, enabling agile and non-deterministic quantum circuits [13]. Other CDU components are also well-developed, though tailored for specific tasks. Several decoding algorithms such as Union-find [31], minimum-weight-perfect-matching (MWPM) [30], and neural-network decoders [34] were already implemented in FPGA [41] or dedicated hardware [42], [43], achieving an average decoding latency per round of below 1 microsecond. In addition, small decoding tasks benefit from a look-up table decoder [33] which can be implemented directly in the controller, while large decoding tasks might leverage parallelizable algorithm such as fusion blossom [35], which are suitable for GPU implementation. Finally, an essential aspect of the CDU that affects its performance is its microarchitecture (its detailed and dedicated hardware structure). Recent studies have shown that a well-designed decoder microarchitecture can overcome assumed decoding tradeoffs, reaching fast, accurate and scalable performance [42]. Novel controller microarchitectures have been proposed to optimize and enable scalable QEC control [44]. Altogether, the diversity of each component highlights the need for a holistic CDU benchmark.

IV. THE ROLE OF FEED-FORWARD LATENCY IN QEC QUANTUM COMPUTATION

In Section II, we discussed the necessity of conditional decoding-dependent feed-forward for implementing a T gate with surface codes. This requirement extends to the implementation of any non-Clifford gate in any QEC computation that is measurement-based, for example in [25]. A critical question arises: what are the requirements for feedforward latency (FFL), and what is the impact of excessive latency? This chapter provides a general analysis of FFL under various classical parameters, applicable to any

QEC stabilizer code requiring feed-forward for fault-tolerant quantum computation.

A. THE DEPENDENCIES BETWEEN DECODING TASKS IN NON-CLIFFORD QEC CIRCUITS

To further illustrate the role of feed-forward in fault-tolerant QEC non-Clifford circuits, we analyze a circuit consisting of two consecutive non-commuting non-Clifford gates (Figure 3a) using the limited quantum resources of a single ancillary surface. The surface-level execution of the circuit (Figure 3b) employs the ancillary logical qubit (surface) to implement the non-Clifford gates and their conditional corrections fault-tolerantly. Importantly, since the non-Clifford gates do not commute, the feed-forward of the first gate (T) must be applied before executing the second non-Clifford gate. Thus, the computational logical qubit will remain idle during the decoding of the first logical parity measurement (ZZ lattice surgery) which will determine the initialization state of the ancillary surface, either $|i\rangle=|0\rangle+i|1\rangle$ for the S gate correction or the magic state $|X^{1/4}\rangle=|+\rangle+e^{i\pi/4}|-\rangle$ to start the next non-Clifford gate.

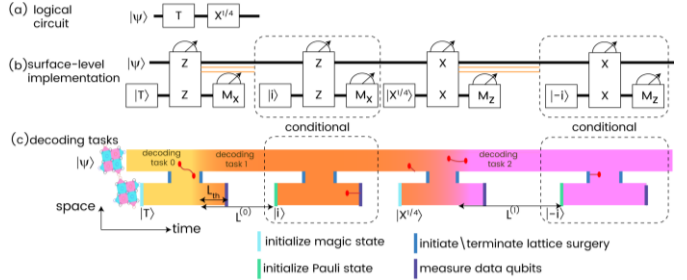


FIGURE 3. Example of non-Clifford computation with surface codes. (a) A logical circuit containing two non-commuting non-Clifford gates. (b) The fault-tolerant logical circuit implementing (a) with surface codes using a single ancillary surface. The dashed square denotes the feed-forward conditional logical gates ensuring the planned circuit is executed. (c) A two-dimensional section of the space-time view of the decoding tasks of the circuit in (b) implemented with surface codes. Colors represent separate decoding tasks, ending each task with a logical measurement which determines a feed-forward operation. The decoding outcome of the lattice surgery between a magic state surface and the computation surface determines a feed-forward circuit. The FFL (L) delays the circuit if it exceeds a threshold latency L_{th} , set by the number of rounds required to establish the measurement result of the ancillary surface. We note that the boundary conditions between decoding tasks are necessary to match (red lines) syndromes (red circles) between tasks. An implementation of a similar logical circuit with additional ancillary surfaces is shown in Figs. S1 and S2.

Figure 3c presents the division of the logical circuit of Figure 3b into different decoding tasks, illustrated in a two-dimensional section of the space-time view of the code, where the space axes correspond to the location of an error event (as Figure 6 in [26]). The first decoding task (task 0, yellow) is responsible for determining the first ZZ measurement outcome. The task starts with the beginning of the circuit. However, its end point is not well-defined since a set of errors might be fully detectable only after the ZZ measurement has ended [26]. As a result, also the beginning of the second decoding task (decoding task 1, orange) should receive some boundary conditions from the first decoding task. This decoding task will determine the feed-forward corresponding to the second non-Clifford gate of the circuit. Importantly, the

size (in term of syndromes to be decoded) of the second decoding task is completely determined by the first decoding task. If the first feed-forward is applied, then the second decoding task will include an additional fixed amount of the syndromes of the S gate correction. Moreover, the second decoding task will have a size that is dependent on the first FFL (denoted as $L^{(0)}$) since the data to be decoded in the second task continues to be acquired during the decoding of the first task. This dependency between tasks highlights the importance of the FFL: a delayed $L^{(0)}$ increases the challenge of the second decoding task, resulting in an increased $L^{(1)}$ and so on. In the analysis below, we explain the requirements on the CDU to avoid such diverging effect.

Not all values of FFL necessarily increase the size of the subsequent decoding task. In Figure 3c, limiting to a single ancillary surface creates a threshold latency L_{th} . If the controller is ready to apply the feed-forward before L_{th} , the FFL will be L_{th} and it will not increase the size of the next decoding task. In this case, the classical controller waits for the ancillary surface measurement before re-initializing it. Here, L_{th} is determined by d stabilizer rounds needed for a fault-tolerant surface measurement. A similar L_{th} value appears when using two ancillary surfaces [25] (see SI section 2 and Figures S1, S2). More generally, every non-Clifford circuit and number of ancillary surfaces will determine a different L_{th} for each decoding task (For example, $L_{th}=0$ in the circuit from Figure 1c).

The example circuit shows magic states prepared in a single surface-level timestamp (d stabilizer rounds), typical with non-fault-tolerant state injection [27], [28]. A noisy magic state can suffice for shallow non-Clifford logical circuits or for magic state distillation circuits[39]. This process outputs a low-error logical initialization using many noisy magic state initializations (at least 15 for the 15-to-1 distillation process) and in a qubit-limited case (e.g., in [25]) include also non-Clifford gates which requiring feed-forward. Therefore, the magic-state distillation circuit includes a similar connection and dependencies between decoding tasks as in Figure 3, and our analysis and benchmarks below will also assess the CDU's capability to run a magic-state distillation procedure.

B. ANALYSIS OF THE CDU SYSTEM CAPABILITY TO EXECUTE NON-CLIFFORD CIRCUITS

We established that non-Clifford quantum computation with QEC consists of dependent decoding tasks, where one task's FFL determines the next task's size. This section explains the CDU's required properties for running non-Clifford circuits on a given quantum system, showing how these properties lead to qualitatively different operation regimes that determine the feasibility of logical quantum computation. To elucidate the origins of the various regimes, we conduct a dynamical system analysis [45]. The CDU behavior is considered dynamical since the FFL of decoding task n , $L^{(n)}$, is connected to $L^{(n-1)}$ through the number of syndromes that the decoder is required

to analyze in task n , $N^{(n)}$. This connection motivates using the broad toolset of dynamical system analysis to derive the CDU's behavior for a given quantum system, with variables $N(L)$, the number of syndromes the quantum computer generates for a given a FFL, and $L(N)$, the FFL of the CDU given the number of syndromes.

Figures 4a-b show examples of using dynamical system analysis to derive the CDU's behavior, with a linear decoder (blue line in Figure 4a), where decoding time is linearly dependent to the number of syndromes, and a varying complexity decoder (red curve in Figure 4b). The system's initial state (that includes N_0 syndromes) evolves (arrows) until reaching a stable steady-state point where the curves of $L(N)$ and $N(L)$ (purple curve in Figures 4a,b) intersect at a steady-state FFL (L_{ss}). This point determines the time required to fully execute a each non-Clifford gate when the system reaches its steady-state operation point. Moreover, since the logical error depends on the size of the decoding task, $N(L_{ss})$, the steady-state point will eventually determine the logical circuit fidelity since the logical coherence depends on the number of stabilizer rounds in the surface idling [14].

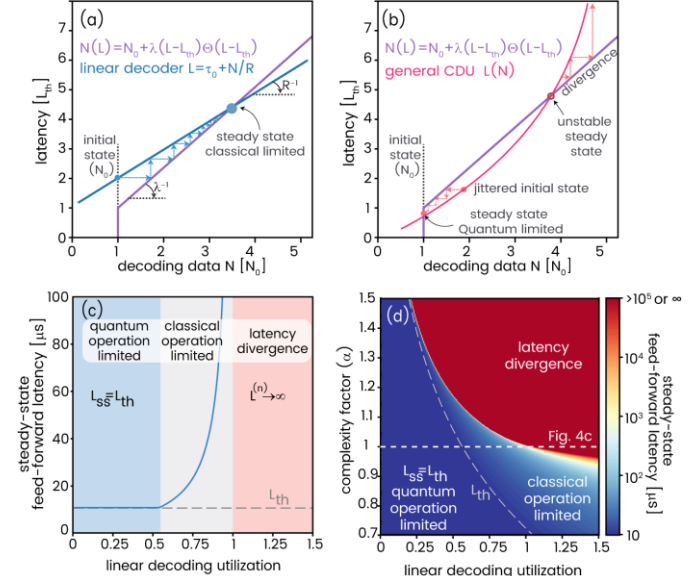


FIGURE 4. Simulations of the feed-forward latency, its steady-state, and the CDU computation regimes. (a-b) A dynamical system analysis for a linear decoder (a) and a general decoder (b), presenting the dynamics of the system using the curves of $L(N)$ (blue and red) and $N(L)$ (purple) from the initial state of $L(N_0)$ until reaching a steady-state when the curves intersect. The steady-state latency can show a quantum-limited operation when converging to L_{th} , classical limited operation when the steady-state is stable and above L_{th} , or a latency diverging regime when the intersection does not exist or when the FFL is larger than an unstable steady-state point. **(c-d)** The steady-state FFL for a linear decoding model (c) or for different decoding parameters (d). All simulation parameters are presented in Table S1, and latency plots for various values of L_{th} are presented in Figure S3.

The L_{ss} value determines three conceptually different operation regimes. (i) classical-operation limited regime, where the system reaches a stable steady-state FFL larger than the threshold latency ($L_{ss} > L_{th}$). In this regime (Figure 4a), the CDU latency limits the quantum computation logical clock, but can still enable many non-Clifford gates. (ii) quantum-operation limited regime, where the steady-state FFL equals the threshold latency ($L_{ss} = L_{th}$), as the stable steady-state point

in Figure 4b. In this regime the calculation time depends solely on the quantum operations. (iii) latency divergence regime, where the FFL will continuously increase, making scalable quantum computation infeasible, as $\lim_{n \rightarrow \infty} L^{(n)} \rightarrow \infty$, shown in the unstable steady-state point in Figure 4b.

The operation regime can be derived using the following analysis. Consider a quantum system generating decoding data at a rate λ (syndromes per second), leading to a linear connection $N^{(n)}(L^{(n-1)}) = N_0 + \lambda(L^{(n-1)} - L_{th})\Theta(L^{(n-1)} - L_{th})$, with N_0 denotes a the number of syndromes when the FFL is L_{th} (which for simplicity we assume independent in n) and $\Theta()$ is a step function. Then, we can examine a linear latency model $L(N) = \tau_0 + N/R$, with throughput rate R in decoded syndromes per second, and τ_0 for the decoder-controller communication and decoder bring-up latencies. Figure 4a shows that this linear system can reach the steady-state point only if the slope of $L(N)$ is smaller than the slope of $(N(L))^{-1}$, i.e., if $\lambda/R < 1$. This ratio describes the decoder's utilization $U = \lambda/R$, indicating the syndrome generation rate from a quantum system over the decoding throughput. Figure 4c shows L_{ss} as a function of U (calculated analytically in SI section S3) for a linear decoder. When $L(N_0) > L_{th}$, the steady-state latency grows with the utilization and diverge as the utilization approaches 1. When $U > 1$ (red-zone), the latency diverges so that the classical behavior prevents any quantum calculation. Conversely, when $L(N_0) < L_{th}$ (and $U < 1$), reducing U does not change L_{ss} corresponding to an intersection when $N(L)$ is vertical in Figure 4a.

For a general CDU latency behavior (Figure 4b), the system will converge into a stable steady-state if $U(N) = \lambda/R(N) < 1$ for all N , with the throughput rate dependent on N via $R(N) = (\partial L(N)/\partial N)^{-1}$. If $U > 1$ at the intersection point the steady state is unstable and will cause latency divergence once a single FFL is higher than the unstable point. Realistic decoders show an expected FFL behavior of the form $L(N) = \tau_0 + \tau_1 N^\alpha$ (e.g., [35], [43], [46]), where α is the complexity factor of the decoder, and τ_1 is a pre-factor, making $\lambda\tau_1$ the linear decoder utilization. Figure 4d shows the steady-state FFL under variation of the complexity and the linear decoder utilization, emphasizing the importance of near-linear complexity decoding algorithms to avoid latency divergence.

Overall, using dynamical system analysis and graphical representations enable an intuitive analysis of the operational boundaries for CDU with any quantum hardware and QEC codes. These examples can extend to assess system dynamics amid significant latency or syndrome fluctuations, employing a probabilistic methodology to examine latency divergence likelihood. The dynamical-system approach is applicable to any non-linear behaviors of $N(L)$ and $L(N)$, correlative connections between the two, and cases where L_{th} varies between decoding tasks. In these cases, the existence and value of a stable steady-state FFL will determine the CDU's capability for useful quantum computation.

V. CDU BENCHMARKS: STEADY-STATE FEED-FORWARD LATENCY

After recognizing the pivotal influence of classical control and computational performance on fault-tolerant QEC computations, we propose two benchmarks aimed at evaluating the CDU's capability to support such computations in the near and medium term. These benchmarks focus on latency benchmarking, measuring the time from the last input of measurement signals to the controller until the first decoding-dependent conditional output signal from the controller. Specifically, the duration it takes from a set of measurements that implement a logical measurement until a conditional set of feed-forward operations is performed to implement a logical feed-forward on a logical qubit, based on the error decoding of a logical measurement outcome. Each latency benchmark below relates to a steady-state FFL that encompasses three key aspects in a single parameter: (i) the capacity to simultaneously execute quantum operations alongside the decoding process; (ii) the capability of the CDU to avoid divergence in the decoding task and reach a steady-state point (i.e., good enough decoding throughput); and (iii) the speed of the decoder, the controller, and their integration through the steady-state FFL value.

To create well-defined and rigorous benchmarks, we focus on a specific representative configuration: a QEC rotated surface code of distance-5 and distance-11 with a stabilizer round cycle time of 1 microsecond, a union-find decoding algorithm [31], physical error rates of 0.5% (two-qubit depolarization and single-qubit measurement), and a logical circuit that is uniquely defined in each of the two benchmarks below. We define logical circuits simple enough to keep the benchmarks implementable in the near term, using only Clifford gates and with a logical Pauli feed-forward which should occur after every decoding task. We require each physical measurement within the logical gates to be randomly generated RF (radio-frequency) pulses according to the error model so that the benchmark will include the signal processing involved in typical superconducting transmon state estimation (demodulation, integration, and threshold-based discrimination). The benchmarks can then be evaluated using the CDU only, without a connection to quantum hardware.

This representative use case pushes the classical hardware to the limit since superconducting qubits have the fastest clock cycle today. We believe that these benchmarks are relevant even for the slower implementations, as we expect gate times to drop as the field progresses. Finally, we define a specific decoding algorithm, which we chose as a representative of the widely used minimum-weight-perfect-matching variants. It is important to predefine a decoding algorithm for the benchmarks so that different CDUs would perform a similar classical calculation, i.e., will generate the same output given a similar input.

A. NEAR-TERM BENCHMARK: STEADY-STATE INTER-CIRCUIT FEED-FORWARD LATENCY (SIFL)

The first benchmark is based on a preliminary use-case in which the quantum resources are limited to a single logical qubit. Although a single surface is not sufficient for performing quantum computation, this benchmark stands as a first step towards the scalability of QEC quantum computation, suitable for checking the CDU capabilities with available decoding algorithms. The logical circuit implemented in the benchmark is shown in Figure 5a. The controller initializes the surface (data qubits) in the $|0\rangle$ state, performs 10 stabilizer rounds, and then measures the data qubits. The benchmark clock starts once the last sample of the last data qubit measurement signal is sampled by the controller (cf. the measurement timestamp in [13]). The controller then immediately initializes the surface for the next circuit followed by execution of repeated stabilizer rounds until the decoding of the first circuit is done. Then, the controller applies the appropriate conditional feedback based on the decoded frame and measures the surface again. We measure latency of the first decoding task, denoted by $L^{(0)}$, as the time from the start of the benchmark clock until the first sample of the conditional pulse is played from the controller (cf. the conditional pulse timestamp in [13]). To further verify the scalability of the classical hardware, we do not stop the benchmark once the first FFL is measured (related to the decoding of 10 stabilizer rounds). We set the end of the benchmark to be the *steady-state FFL*. We define steady-state stopping condition as $(L^{(n)} - L^{(n-1)})/L^{(n)} < 0.05$ where $L^{(n)}$ relates to an unknown decoding task (n) , which contains an unknown number of stabilizer rounds. To avoid irregularities, we define the benchmark as the average of 1000 shots for which $L^{(n)}$ is found. Lastly, we define the size of the surface for the benchmark to be surface 49 (distance-5) or surface 241 (distance-11), and refer to these benchmarks as Steady-state Inter-circuit FFL 49 or 241, or in short, the SIFL-49 or SIFL-241 benchmarks.

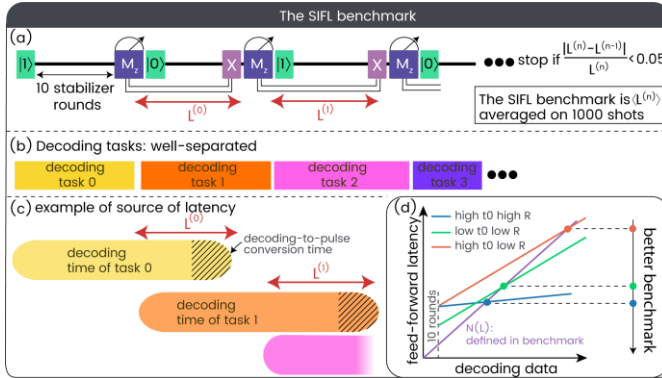


FIGURE 5. The Stead-state Inter-circuit Feed-forward Latency (SIFL) benchmark. (a) Logical circuit for measuring the SIFL benchmark. The double line represents a decoding-dependent conditional gate, and the red arrow represents the experimental FFL of the first two decoding tasks. The number of circuits is determined by the stopping condition. The SIFL benchmark is the FFL of the last circuit, averaged over 1000 repetitions. (b) The decoding task view of the SIFL benchmark, where each decoding task is strictly separated from the other decoding tasks. The data for the first decoding task (yellow) is predetermined in the benchmark as 10 stabilizer rounds, while the number of stabilizer rounds in all other decoding tasks is determined by the previous FFL

$(L^{(n-1)})$. (c) Example of the source of FFL, which includes both the decoding time and the time to convert the decoding results into a feed-forward pulse (dashed). (d) Qualitative example of different benchmark outcomes when comparing CDUs according to their latency offset τ_0 and throughput rate R .

The concrete definition of the SIFL benchmark is shown in Listing 1 as a pseudocode. We write the variables and building block commands required to run a single-surface experiment and measure the benchmark. The pulse-level statements and macros “**initialize surface**”, “**play**”, “**stabilizer round**”, and “**measure surface**” include a set of predefined physical RF pulses and measurements that are detailed in Listing S1 and are compatible with the representative use case discussed above. To create the separation between the classical hardware that we want to benchmark and the quantum hardware (that is, to be able to benchmark the classical hardware without quantum hardware), we add as an input to these operations the predefined parameters **error_probability** and **round_time** for the stabilizer round that we can control classically in the analogue input to the controller. Apart from the analog signals, we write the controller-decoder communication commands (Cyan) and decoding algorithm (mustard) explicitly. During the decoding, the controller is required to execute stabilizer rounds for an unknown number of rounds, described by the **while** loop. Thus, classical data is acquired during the decoding process. Interestingly, although we aim for a surface code, the pseudocode in Listing 1 can be used to benchmark any QEC stabilizer code.

```

rounds = 10
error_probability = 0.005
round_time = 1E-6 #microsecond
latency_limit = 1 #second
averaging_loop = 1000
decoding_algorithm = Union_find
send_to_decoder(algorithm=decoding_algorithm)
SIFL_of_sample = []
initialize_simulation(error_probability, round_time)
for i in range(averaging_loop):
    task_idx = 0
    task_latency = [latency_limit]
    initialize_surface(q0, state=1)
    for j in range(rounds):
        ancilla_bits = stabilizer_round()
        send_to_decoder(ancilla_bits, task = task_idx)
        data_bits = measure_surface(q0, timestamp->tic)
        send_to_decoder(data_bits, task = task_idx)
        while task_latency[-1] < latency_limit:
            task_idx += 1
            initialize_surface(q0, state=1+ task_idx mod 2)
            [logical_result, decoding_recieved] = get_decoding_result(task= task_idx -1)
            while not decoding_recieved:
                ancilla_bits = stabilizer_round()
                send_to_decoder(ancilla_bits, task = task_idx)
                [logical_result, decoding_received] = get_decoding_result(task= task_idx -1)
            play_x(q0, timestamp-> toc)
            task_latency.append(toc- tic)
            if abs(task_latency[-1]- task_latency[-2])<0.05* task_latency[-1] :
                SIFL_of_sample.append(task_latency[-1])
                break
            data_bits = measure_surface(q0, error_probability, timestamp->tic)
SIFL = mean(SIFL_of_sample)

```

Listing 1: Pseudocode for measuring the Stead-state Intercircuit Feed-forward Latency. **Green:** elements of the configuration file. **Blue:** real-time classical variables. **Red:** pulse-level commands. **Orange:** pre-defined constants and functions. **Bright Purple:** control flow statement. **Cyan:** controller-decoder communication statement. **Mustard:** decoding algorithm. We note that the macros “**stabilizer_round**”, “**initialize_surface**”, and “**measure_surface**” are defined in Listing S1.

The SIFL benchmark simplifies the requirements compared to those needed for non-Clifford gates due to the distinct separation between decoding tasks, as shown in Figure 5b. This separation allows the SIFL benchmark to be executable with various decoding algorithms, which typically require well-defined boundaries (initialization and logical measurement). Nonetheless, an important property to evaluate is the decoder's ability to start processing before the circuit ends and to run several decoding tasks in parallel, as shown in Figure 5c. In this illustration, we demonstrate a scenario where decoding completes shortly after the task acquisition ends. This is possible because decoding began before the task acquisition concluded, resulting in latency being primarily influenced by the conversion of the decoding results into a feed-forward pulse (e.g., due to decoder-controller communication). If decoding were to start only after the task acquisition ends, it would increase the latency offset τ_0 , thereby raising the benchmark value (see green and orange lines in Figure 5d). A high τ_0 can potentially result in a better benchmark, but only when using a decoder with high throughput rate R (as shown by the blue line in Figure 5d). This qualitative figure demonstrates how the dynamical system diagram is used to establish the benchmark, where a better benchmark corresponds to a smaller steady-state FFL value. We expect that these values would take the order of magnitude of few microseconds at the best case to milliseconds and a non-converging value for unsatisfiable CDU systems.

B. MEDIUM-TERM BENCHMARK: STEADY-STATE SURGERY FEED-FORWARD LATENCY (SSFL)

To provide a benchmark that confronts the most demanding part for running non-Clifford circuits in terms of real-time decoding, we define a second benchmark. In this benchmark, we modify the SIFL benchmark so that the logical measurement will be a lattice surgery rather than a single surface measurement, as shown in Figure 6 and defined in Listing 2. The lattice surgery feed-forward is one of the main building blocks for performing non-Clifford gates (also in color codes [47]), and moreover, is the only type of feed-forward required for the entire quantum circuit. As in the previous benchmark, we evaluate the decoding throughput, the classical-quantum parallelization, and the speed of the overall integration, by defining the benchmark as a Steady-state Surgery FFL (SSFL). Each latency is defined from the moment one lattice surgery ends (where each surgery has d stabilizer rounds) until the moment the corresponding feed-forward is applied, while the stopping condition and averaging is similar to the SIFL benchmark. In this case, we define the benchmark for a distance-3 or distance-5 configuration with a single data qubit column (as in Figure 1b), containing 41 or 111 physical qubits.

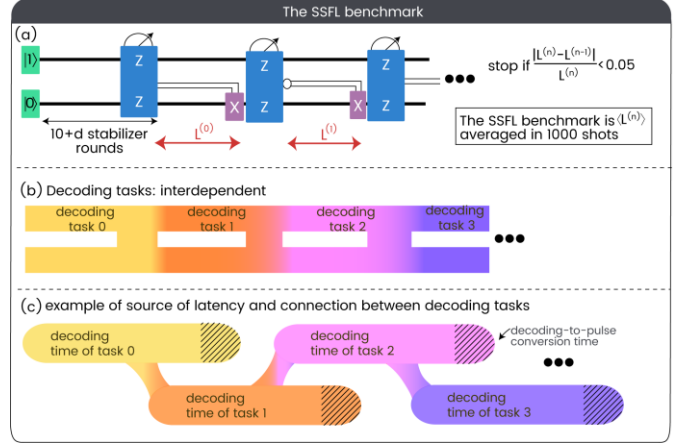


FIGURE 6. The Stead-state Surgery Feed-forward Latency (SSFL) benchmark. (a) Logical circuit for measuring the SSFL benchmark. The $\text{I}(\text{I})$ represents a conditional gate, and the red arrows represent the FFL of the first two decoding tasks where each decoding task ends with the termination of the lattice surgery. The number of decoding tasks is determined by the stopping condition. The SSFL benchmark is the feed-forward latency of the last decoding tasks, averaged by 1000 shots. The stabilizer rounds are not shown since they represent a logical identity. (b) The decoding task view of the SSFL benchmark, where each decoding task is not strictly separated from the other decoding tasks. (c) Example of the source of FFL, and the connection between the tasks where there is a continuation and correlation in the data of each decoding task.

```

rounds = 10
surgery_rounds = d
error_probability = 0.005
round_time = 1E-6 #microsecond
latency_limit = 1 #second
averaging_loop = 1000
decoding_algorithm = Union_find
send_to_decoder(algorithm=decoding_algorithm)
initialize_simulation(error_probability, round_time)
SSFL_of_sample = []
for i in range(averaging_loop):
    task_indx = 0
    task_latency = [latency_limit]
    initialize_surface(q0, state=1)
    initialize_surface(q1, state=0)
    for i in range(rounds):
        ancilla_bits = stabilizer_round()
        send_to_decoder(ancilla_bits, task = task_indx)
        while task_latency[-1]< latency_limit:
            initialize_surgery(q0, q1)
            for i in range(surgery_rounds):
                ancilla_bits = stabilizer_round()
                send_to_decoder(ancilla_bits, task = task_indx)
            surgery_data_bits = terminate_surgery((q0, q1), timestamp->tic)
            send_to_decoder(surgery_data_bits, task = task_indx)
            task_indx = task_indx + 1
            [logical_result, decoding_received]=get_decoding_result(task=task_indx -1)
            while not decoding_received:
                ancilla_bits = stabilizer_round()
                send_to_decoder(ancilla_bits, task=task_indx)
            [logical_result, decoding_received]=get_decoding_result(task=task_indx -1)
            play_x(q1, timestamp->toc)
            task_latency.append(toc- tic)
            if abs(task_latency[-1]-task_latency[-2])<0.05* task_latency[-1]:
                SSFL_of_sample.append(task_latency[-1])
                break
SSFL=mean(SSFL_of_sample)

```

Listing 2: Pseudocode for measuring the Stead-state Surgery Feed-forward Latency (SSFL). Color coding is the same as in Listing 1, the macros `initialize_surgery` and `terminate_surgery` are defined in Listing S1.

As in the SIFL benchmark, the SSFL benchmark also includes idling stabilizer rounds until the feed-forward is applied (see Figure 3a and Listing 2), so that the latency of the first decoding task will determine the amount of processing data of the second decoding task. However, a significant difference

between the two benchmarks comes from the fact that the decoding tasks are not well-separated, as we show in Figures 6b and 6c. The second decoding task will depend on the syndromes from the first decoding task, or other boundary conditions that are transferred between decoding tasks to overcome a set of errors with syndromes in both tasks (illustrated by the connection between the tasks). As a result, we expect an additional demand on the CDU when implementing the SSFL benchmark compared to the SIFL benchmark, which will result in a latency expansion and an overall worse benchmark value. Finally, the biggest challenge in implementing this benchmark is that to the best of our knowledge, it is currently impossible with the available decoding tools (such as PyMatching [36] or Fusion-Blossom [35]) to have a dependency between decoding tasks which share correlated syndromes. Hence, executing the SSFL benchmark will necessitate algorithmic development alongside control hardware improvements.

VI. DISCUSSION

In this manuscript, we have explained the central roles of the CDU, the necessity for a low FFL, and suggested two benchmarks for evaluating the CDU performance. The suggested benchmarks provide a first reduction of all CDU components into few holistic evaluation numbers. Although these benchmarks do not perform any useful quantum calculations, they are defined using representative configurations according to current state-of-the-art parameters. Moreover, they verify the ability of the CDU to support future state-of-the-art QEC experiments, setting the stage for scaling quantum hardware. These benchmarks, the commands within the pseudocodes, and the operation regime analysis, are general for most other QEC stabilizer codes which may have a different detailed physical pulse sequence and decoding algorithms. Eventually, these benchmarks or intended to enable real-time decoding with the highest performance in novel near-term QEC experiments with available quantum hardware.

In the long term, we expect a dominant role in parallelizing classical calculations in the CDU. The controlling system will need to parallelize many decoding tasks to keep track of the frame of each logical qubit, and then merge decoding tasks during multi-surface lattice surgeries. Schemes to optimize the number of decoding tasks compared to the number of logical qubits in various algorithms was recently suggested [48]. In addition, it would be beneficial to consider indirect benchmarks for evaluating a QEC operation runtime, including the time it takes to run multiple shots, to compile logical circuits into T-gate operations [49], and to load the circuit parameters (e.g., to synthesize circuit waveform sequences). In this context, an interesting benchmark will be the time it takes to perform embedded calibrations for the circuit parameters optimization (e.g., [50], [51], [52]). The quality of the optimization will eventually determine the physical error probability of the circuit which in turn gives rise

to another possible set of benchmarks related to the decoder adaptation time. The decoder will be required to adapt its weights and estimates of the circuit noise (for example by using optimal noise estimation [53]) and to adapt to catastrophic events [54], [55].

We foresee that optimizing for the benchmarks that we defined here while keeping high decoding accuracy will be at the core of quantum computation utility. Once the surgery latency is minimized, the effort will move towards minimizing the multi-surface surgery latency, and eventually the magic state distillation time. The distillation time is expected to determine de facto the whole quantum computation time for surface-code-based computation, which is currently the main expected route for reducing dramatically logical error rates. Finally, even if other promising QEC codes such as QLDPC codes [56] or other unique codes [57] will become dominant, all properties and blueprints for CDU that we describe here will still stand. Thus, having clear benchmarks that combine the complete requirements of a CDU is a vital and fundamental component in the development of quantum computing.

ACKNOWLEDGMENT

This publication has received funding under Horizon Europe programme HORIZON-CL4-2021-DIGITAL-EMERGING-01-30 via the project 101070144 (EuRyQa).

REFERENCES

- [1] P. W. Shor, “Fault-tolerant quantum computation,” in *Proceedings of 37th Conference on Foundations of Computer Science*, Burlington, VT, USA: IEEE Computer Society, 1996, pp. 56–65. doi: 10.1109/SFCS.1996.548464.
- [2] E. Knill, R. Laflamme, and W. H. Zurek, “Resilient Quantum Computation: Error Models and Thresholds,” *Proc. R. Soc. Lond. Ser. Math. Phys. Eng. Sci.*, vol. 454, no. 1969, pp. 365–384, Jan. 1998, doi: 10.1098/rspa.1998.0166.
- [3] R. P. Feynman, “Simulating physics with computers,” *Int. J. Theor. Phys.*, vol. 21, no. 6–7, pp. 467–488, Jun. 1982, doi: 10.1007/BF02650179.
- [4] P. W. Shor, “Polynomial-Time Algorithms for Prime Factorization and Discrete Logarithms on a Quantum Computer,” *SIAM J. Comput.*, vol. 26, no. 5, pp. 1484–1509, Oct. 1997, doi: 10.1137/S0097539795293172.
- [5] D. Gottesman, “Stabilizer Codes and Quantum Error Correction,” Caltech, 1997.
- [6] J. Preskill, “Reliable Quantum Computers,” *Proc. R. Soc. Lond. Ser. Math. Phys. Eng. Sci.*, vol. 454, no. 1969, pp. 385–410, Jan. 1998, doi: 10.1098/rspa.1998.0167.
- [7] E. T. Campbell, B. M. Terhal, and C. Vuillot, “Roads towards fault-tolerant universal quantum computation,” *Nature*, vol. 549, no. 7671, pp. 172–179, Sep. 2017, doi: 10.1038/nature23460.
- [8] A. deMarti iOlius, P. Fuentes, R. Orús, P. M. Crespo, and J. E. Martinez, “Decoding algorithms for surface codes,” Jul. 27, 2023, *arXiv*: arXiv:2307.14989. Accessed: Jul. 31, 2023. [Online]. Available: <http://arxiv.org/abs/2307.14989>

[9] N. Ofek *et al.*, “Extending the lifetime of a quantum bit with error correction in superconducting circuits,” *Nature*, vol. 536, no. 7617, pp. 441–445, Aug. 2016, doi: 10.1038/nature18949.

[10] D. Devulapalli, E. Schoute, A. Bapat, A. M. Childs, and A. V. Gorshkov, “Quantum Routing with Teleportation,” Apr. 08, 2022, *arXiv: arXiv:2204.04185*. Accessed: Oct. 30, 2023. [Online]. Available: <http://arxiv.org/abs/2204.04185>

[11] E. Bäumer *et al.*, “Efficient Long-Range Entanglement using Dynamic Circuits,” Aug. 24, 2023, *arXiv: arXiv:2308.13065*. Accessed: Oct. 30, 2023. [Online]. Available: <http://arxiv.org/abs/2308.13065>

[12] M. Foss-Feig *et al.*, “Experimental demonstration of the advantage of adaptive quantum circuits,” Feb. 06, 2023, *arXiv: arXiv:2302.03029*. Accessed: Jul. 04, 2023. [Online]. Available: <http://arxiv.org/abs/2302.03029>

[13] L. Ella *et al.*, “Quantum-classical processing and benchmarking at the pulse-level,” Mar. 07, 2023, *arXiv: arXiv:2303.03816*. Accessed: Jul. 05, 2023. [Online]. Available: <http://arxiv.org/abs/2303.03816>

[14] Google Quantum AI *et al.*, “Suppressing quantum errors by scaling a surface code logical qubit,” *Nature*, vol. 614, no. 7949, pp. 676–681, Feb. 2023, doi: 10.1038/s41586-022-05434-1.

[15] D. Bluvstein *et al.*, “Logical quantum processor based on reconfigurable atom arrays,” *Nature*, Dec. 2023, doi: 10.1038/s41586-023-06927-3.

[16] A. Wack *et al.*, “Quality, Speed, and Scale: three key attributes to measure the performance of near-term quantum computers,” Oct. 28, 2021, *arXiv: arXiv:2110.14108*. Accessed: Jul. 05, 2023. [Online]. Available: <http://arxiv.org/abs/2110.14108>

[17] F. Battistel *et al.*, “Real-time decoding for fault-tolerant quantum computing: progress, challenges and outlook,” *Nano Futur.*, vol. 7, no. 3, p. 032003, Sep. 2023, doi: 10.1088/2399-1984/aceba6.

[18] B. M. Terhal, “Quantum Error Correction for Quantum Memories,” *Rev. Mod. Phys.*, vol. 87, no. 2, pp. 307–346, Apr. 2015, doi: 10.1103/RevModPhys.87.307.

[19] E. Dennis, A. Kitaev, A. Landahl, and J. Preskill, “Topological quantum memory,” *J. Math. Phys.*, vol. 43, no. 9, pp. 4452–4505, Sep. 2002, doi: 10.1063/1.1499754.

[20] A. G. Fowler, M. Mariantoni, J. M. Martinis, and A. N. Cleland, “Surface codes: Towards practical large-scale quantum computation,” *Phys. Rev. A*, vol. 86, no. 3, p. 032324, Sep. 2012, doi: 10.1103/PhysRevA.86.032324.

[21] D. Horsman, A. G. Fowler, S. Devitt, and R. Van Meter, “Surface code quantum computing by lattice surgery,” *New J. Phys.*, vol. 14, no. 12, p. 123011, Dec. 2012, doi: 10.1088/1367-2630/14/12/123011.

[22] D. Litinski and F. von Oppen, “Lattice Surgery with a Twist: Simplifying Clifford Gates of Surface Codes,” *Quantum*, vol. 2, p. 62, May 2018, doi: 10.22331/q-2018-05-04-62.

[23] A. G. Fowler and C. Gidney, “Low overhead quantum computation using lattice surgery,” Aug. 30, 2019, *arXiv: arXiv:1808.06709*. Accessed: Jul. 06, 2023. [Online]. Available: <http://arxiv.org/abs/1808.06709>

[24] C. Chamberland and E. T. Campbell, “Universal Quantum Computing with Twist-Free and Temporally Encoded Lattice Surgery,” *PRX Quantum*, vol. 3, no. 1, p. 010331, Feb. 2022, doi: 10.1103/PRXQuantum.3.010331.

[25] D. Litinski, “A Game of Surface Codes: Large-Scale Quantum Computing with Lattice Surgery,” *Quantum*, vol. 3, p. 128, Mar. 2019, doi: 10.22331/q-2019-03-05-128.

[26] O. Higgott, T. C. Bohdanowicz, A. Kubica, S. T. Flammia, and E. T. Campbell, “Improved Decoding of Circuit Noise and Fragile Boundaries of Tailored Surface Codes,” *Phys. Rev. X*, vol. 13, no. 3, p. 031007, Jul. 2023, doi: 10.1103/PhysRevX.13.031007.

[27] Y. Li, “A magic state’s fidelity can be superior to the operations that created it,” *New J. Phys.*, vol. 17, no. 2, p. 023037, Feb. 2015, doi: 10.1088/1367-2630/17/2/023037.

[28] C. Gidney, “Cleaner magic states with hook injection,” Feb. 23, 2023, *arXiv: arXiv:2302.12292*. Accessed: Jul. 04, 2023. [Online]. Available: <http://arxiv.org/abs/2302.12292>

[29] Y. Ye *et al.*, “Logical Magic State Preparation with Fidelity beyond the Distillation Threshold on a Superconducting Quantum Processor,” *Phys. Rev. Lett.*, vol. 131, no. 21, p. 210603, Nov. 2023, doi: 10.1103/PhysRevLett.131.210603.

[30] V. Kolmogorov, “Blossom V: a new implementation of a minimum cost perfect matching algorithm,” *Math. Program. Comput.*, vol. 1, no. 1, pp. 43–67, Jul. 2009, doi: 10.1007/s12532-009-0002-8.

[31] N. Delfosse and N. H. Nickerson, “Almost-linear time decoding algorithm for topological codes,” *Quantum*, vol. 5, p. 595, Dec. 2021, doi: 10.22331/q-2021-12-02-595.

[32] C. T. Chubb, “General tensor network decoding of 2D Pauli codes,” Oct. 13, 2021, *arXiv: arXiv:2101.04125*. Accessed: Jul. 02, 2023. [Online]. Available: <http://arxiv.org/abs/2101.04125>

[33] P. Das, A. Locharla, and C. Jones, “LILLIPUT: A Lightweight Low-Latency Lookup-Table Based Decoder for Near-term Quantum Error Correction,” Aug. 14, 2021, *arXiv: arXiv:2108.06569*. Accessed: Jul. 02, 2023. [Online]. Available: <http://arxiv.org/abs/2108.06569>

[34] K. Meinerz, C.-Y. Park, and S. Trebst, “Scalable Neural Decoder for Topological Surface Codes,” *Phys. Rev. Lett.*, vol. 128, no. 8, p. 080505, Feb. 2022, doi: 10.1103/PhysRevLett.128.080505.

[35] Y. Wu and L. Zhong, “Fusion Blossom: Fast MWPM Decoders for QEC,” May 14, 2023, *arXiv: arXiv:2305.08307*. Accessed: Jul. 02, 2023. [Online]. Available: <http://arxiv.org/abs/2305.08307>

[36] O. Higgott, “PyMatching: A Python package for decoding quantum codes with minimum-weight perfect matching,” Jul. 12, 2021, *arXiv: arXiv:2105.13082*. Accessed: Jul. 02, 2023. [Online]. Available: <http://arxiv.org/abs/2105.13082>

[37] C. Gidney, “Stim: a fast stabilizer circuit simulator,” *Quantum*, vol. 5, p. 497, Jul. 2021, doi: 10.22331/q-2021-07-06-497.

[38] J. Haah and M. B. Hastings, “Codes and Protocols for Distilling $\$T\$$, controlled- $\$S\$$, and Toffoli Gates,” *Quantum*, vol. 2, p. 71, Jun. 2018, doi: 10.22331/q-2018-06-07-71.

[39] D. Litinski, “Magic State Distillation: Not as Costly as You Think,” *Quantum*, vol. 3, p. 205, Dec. 2019, doi: 10.22331/q-2019-12-02-205.

[40] D. Gottesman, “The Heisenberg Representation of Quantum Computers,” Jul. 01, 1998, *arXiv*: arXiv:quant-ph/9807006. Accessed: Jul. 04, 2023. [Online]. Available: <http://arxiv.org/abs/quant-ph/9807006>

[41] N. Liyanage, Y. Wu, A. Deters, and L. Zhong, “Scalable Quantum Error Correction for Surface Codes using FPGA,” May 15, 2023, *arXiv*: arXiv:2301.08419. Accessed: Jul. 02, 2023. [Online]. Available: <http://arxiv.org/abs/2301.08419>

[42] P. Das *et al.*, “AFS: Accurate, Fast, and Scalable Error-Decoding for Fault-Tolerant Quantum Computers,” in *2022 IEEE International Symposium on High-Performance Computer Architecture (HPCA)*, Seoul, Korea, Republic of: IEEE, Apr. 2022, pp. 259–273. doi: 10.1109/HPCA53966.2022.00027.

[43] B. Barber *et al.*, “A real-time, scalable, fast and highly resource efficient decoder for a quantum computer,” Sep. 11, 2023, *arXiv*: arXiv:2309.05558. Accessed: Feb. 14, 2024. [Online]. Available: <http://arxiv.org/abs/2309.05558>

[44] X. Fu, L. Lao, K. Bertels, and C. G. Almudever, “A control microarchitecture for fault-tolerant quantum computing,” *Microprocess. Microsyst.*, vol. 70, pp. 21–30, Oct. 2019, doi: 10.1016/j.micpro.2019.06.011.

[45] K. T. Alligood, T. D. Sauer, and J. A. Yorke, *Chaos: an introduction to dynamical systems*, Repr. in Textbooks in mathematical sciences. New York, NY Heidelberg: Springer, 2010.

[46] O. Higgott and C. Gidney, “Sparse Blossom: correcting a million errors per core second with minimum-weight matching,” Mar. 28, 2023, *arXiv*: arXiv:2303.15933. Accessed: Jul. 02, 2023. [Online]. Available: <http://arxiv.org/abs/2303.15933>

[47] A. J. Landahl and C. Ryan-Anderson, “Quantum computing by color-code lattice surgery,” Jul. 18, 2014, *arXiv*: arXiv:1407.5103. Accessed: Jul. 04, 2023. [Online]. Available: <http://arxiv.org/abs/1407.5103>

[48] S. Maurya and S. Tannu, “Managing Classical Processing Requirements for Quantum Error Correction,” Jun. 26, 2024, *arXiv*: arXiv:2406.17995. Accessed: Oct. 26, 2024. [Online]. Available: <http://arxiv.org/abs/2406.17995>

[49] L. Heyfron and E. T. Campbell, “An Efficient Quantum Compiler that reduces T count,” *Quantum Sci. Technol.*, vol. 4, no. 1, p. 015004, Sep. 2018, doi: 10.1088/2058-9565/aad604.

[50] V. V. Sivak *et al.*, “Real-time quantum error correction beyond break-even,” *Nature*, vol. 616, no. 7955, pp. 50–55, Apr. 2023, doi: 10.1038/s41586-023-05782-6.

[51] C. N. Barrett *et al.*, “Learning-based Calibration of Flux Crosstalk in Transmon Qubit Arrays,” *Phys Rev Appl.*, vol. 20, p. 024070, Aug. 2023, doi: 10.1103/PhysRevApplied.20.024070.

[52] P. V. Klimov *et al.*, “Optimizing quantum gates towards the scale of logical qubits,” *Nat. Commun.*, vol. 15, no. 1, p. 2442, Mar. 2024, doi: 10.1038/s41467-024-46623-y.

[53] T. Wagner, H. Kampermann, D. Bruß, and M. Kliesch, “Optimal noise estimation from syndrome statistics of quantum codes,” *Phys. Rev. Res.*, vol. 3, no. 1, p. 013292, Mar. 2021, doi: 10.1103/PhysRevResearch.3.013292.

[54] M. McEwen *et al.*, “Resolving catastrophic error bursts from cosmic rays in large arrays of superconducting qubits,” *Nat. Phys.*, vol. 18, no. 1, pp. 107–111, Jan. 2022, doi: 10.1038/s41567-021-01432-8.

[55] A. Siegel, A. Strikis, T. Flatters, and S. Benjamin, “Adaptive surface code for quantum error correction in the presence of temporary or permanent defects,” *Quantum*, vol. 7, p. 1065, Jul. 2023, doi: 10.22331/q-2023-07-25-1065.

[56] C. A. Pattison, A. Krishna, and J. Preskill, “Hierarchical memories: Simulating quantum LDPC codes with local gates,” Mar. 08, 2023, *arXiv*: arXiv:2303.04798. Accessed: Jul. 10, 2023. [Online]. Available: <http://arxiv.org/abs/2303.04798>

[57] D. Ruiz, J. Guillaud, A. Leverrier, M. Mirrahimi, and C. Vuillot, “LDPC-cat codes for low-overhead quantum computing in 2D,” Feb. 06, 2024, *arXiv*: arXiv:2401.09541. Accessed: Apr. 21, 2024. [Online]. Available: <http://arxiv.org/abs/2401.09541>